AD-A180 270 PI2 PULSATIONS AND THE WESTWARD TRAVELING SURGE IN THE MAGNETOSPHERE - IONOSPHERE COUPLING(U) ALASKA UNIV FAIRBANKS GEOPHYSICAL INST J R KAN NOV 86 1/1

UNCLASSIFIED AFGL-TR-86-0244 F19628-85-K-0012 F/G 4/1 NL

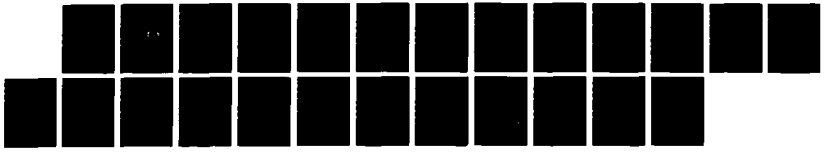

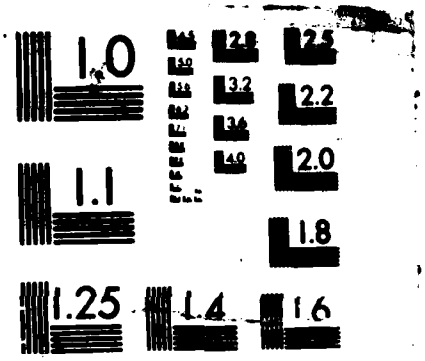

MICROCOPY RESOLUTION TEST CHART
NATIONAL BUREAU OF STANDARDS 1963-A

(12)

AFGL-TR-86-0244

Pi2 Pulsations and the Westward Traveling Surge in the Magnetosphere - Ionosphere Coupling

J. R. Kan

University of Alaska
Geophysical Institute
Fairbanks, Alaska 99775-0800

November 1986

Final Report
15 November 1985 - 30 September 1986

AIR FORCE GEOPHYSICAL LABORATORY
AIR FORCE SYSTEMS COMMAND
UNITED STATES AIR FORCE
HANSCOM AIR FORCE BASE, MASSACHUSETTS 01731

" This technical report has been reviewed and is approved for publication"

PAUL L. ROTHWELL
Contract Manager

NELSON C. MAYNARD
Branch Chief

FOR THE COMMANDER

RITA C. SAGALYN
Division Director

This report has been reviewed by the ESD Public Affairs Office (PA) and is releasable to the National Technical Information Service (NTIS).

Qualified requestors may obtain additional copies from the Defense Technical Information Center. All others should apply to the National Technical Information Service.

If your address has changed, or if you wish to be removed from the mailing list, or if the addressee is no longer employed by your organization, please notify AFGL/DAA, Hanscom AFB, MA 01731. This will assist us in maintaining a current mailing list.

Do not return copies of this report unless contractual obligations or notices on a specific document requires that it be returned.

Unclassified

SECURITY CLASSIFICATION OF THIS PAGE

REPORT DOCUMENTATION PAGE

1a. REPORT SECURITY CLASSIFICATION Unclassified	1b. RESTRICTIVE MARKINGS AD-A180 270
2a. SECURITY CLASSIFICATION AUTHORITY	3. DISTRIBUTION/AVAILABILITY OF REPORT APPROVED FOR PUBLIC RELEASE; DISTRIBUTION UNLIMITED
2b. DECLASSIFICATION/DOWNGRADING SCHEDULE	
4. PERFORMING ORGANIZATION REPORT NUMBER(S)	5. MONITORING ORGANIZATION REPORT NUMBER(S) AFGL-TR-86-0244
6a. NAME OF PERFORMING ORGANIZATION University of Alaska 6b. OFFICE SYMBOL (If applicable)	7a. NAME OF MONITORING ORGANIZATION Air Force Geophysics Laboratory
6c. ADDRESS (City, State and ZIP Code) Geophysical Institute Fairbanks, Alaska 99775-0800	7b. ADDRESS (City, State and ZIP Code) Hanscom AFB Massachusetts 01731
8a. NAME OF FUNDING/SPONSORING ORGANIZATION 8b. OFFICE SYMBOL (If applicable)	9. PROCUREMENT INSTRUMENT IDENTIFICATION NUMBER F19628-85-K-0012
8c. ADDRESS (City, State and ZIP Code)	10. SOURCE OF FUNDING NOS. PROGRAM ELEMENT NO.: 61102F; PROJECT NO.: 2311; TASK NO.: G2; WORK UNIT NO.: HA
11. TITLE (Include Security Classification) Pi2 Pulsations and the Westward Travelling Surge in the Magneto-sphere - Ionosphere Coupling	
12. PERSONAL AUTHOR(S) J.R. Kan	
13a. TYPE OF REPORT Final Report 13b. TIME COVERED FROM 11/15/85 TO 9/30/86	14. DATE OF REPORT (Yr., Mo., Day) 1986 November 15. PAGE COUNT 26
16. SUPPLEMENTARY NOTATION	
17. COSATI CODES FIELD / GROUP / SUB. GR.	18. SUBJECT TERMS (Continue on reverse if necessary and identify by block number) Westward traveling surge; Conductivity profiles; Alfven waves; Magnetosphere-Ionosphere coupling;

19. ABSTRACT (Continue on reverse if necessary and identify by block number)

The dynamics of the westward travelling surge (WTS) is studied in a magnetosphere-ionosphere coupling model. It is shown that the motion of the WTS is governed by the combined effects of the magnetospheric Alfven time scale and the ionospheric recombination time scale. The surge is found to move at variable speeds: the speed is around 6 km/sec westward and less than 1 km/sec northward near the onset of the surge; thereafter, it oscillates irregularly and decreases toward zero. The polar cap potential difference is found to oscillate irregularly as it increases toward the enhanced convection level. The irregular oscillations found in our results are believed to be a general property of multi-time-scale problems.

20. DISTRIBUTION/AVAILABILITY OF ABSTRACT UNCLASSIFIED/UNLIMITED ☐ SAME AS RPT ☒ DTIC USERS ☐	21. ABSTRACT SECURITY CLASSIFICATION Unclassified
22a. NAME OF RESPONSIBLE INDIVIDUAL Paul L. Rothwell	22b. TELEPHONE NUMBER (Include Area Code) 22c. OFFICE SYMBOL AFGL/PHG

DD FORM 1473, 83 APR EDITION OF 1 JAN 73 IS OBSOLETE

Unclassified

SECURITY CLASSIFICATION OF THIS PAGE

TABLE OF CONTENTS

1. Introduction

Magnetosphere and ionosphere interact electromagnetically by means of the field-aligned current and the convection electric field (Vasyliunas, 1972). Recent progress (Kan and Sun, 1985) shows that most of the *substorm phenomena* (Akasofu, 1968) can be understood as manifestations of an enhancement of magnetospheric convection. These include:

(i) The formation of the Harang discontinuity in the convection electric field;

(ii) The intensification of field-aligned currents in the substorm current wedge;

(iii) The rapid motion of auroral forms in the westward traveling surge;

The purpose of this report is to summarize our present understanding of these diverse and complicated substorm phenomena within the framework of magnetosphere-ionosphere (M-I) coupling. Motion of the westward traveling surge (WTS) has been shown to depend on the magnetospheric Alfvén time scale by Kan and Sun (1985) and on the ionospheric recombination time scale by Rothwell et al. (1984). The speeds of the WTS determined from the ionospheric time scale are generally higher than the speeds of the WTS based on the magnetospheric time scale. From these studies, it is evident that the motion of the westward traveling surge must be governed by the combined effects of the magnetospheric and the ionospheric time scales obtained from a global model. The present model is an extension of the magnetosphere-ionosphere coupling model of Kan and Sun (1985), by including the ionospheric recombination time scale in the original model. This is accomplished by replacing the time-independent continuity equation with the time-dependent continuity equation for the ionization

in the ionosphere. It is found that the head of the WTS moves at variable speeds. The surge speed is relatively high at the beginning and then slows irregularly to a standstill. Moreover, the polar cap potential defference is found to oscillate irregularly as it increases.

2. Model

In the interest of time and space, we will concentrate on the formulation of the extension, leaving the rest of the formulation to the original paper by Kan and Sun (1985). The enhanced conductivity in the original model is determined from the time-independent continuity equation. In the present model, the conductivity enhancement is determined from the time-dependent continuity equation for the electron number density in the ionosphere, i.e.,

$$\frac{\partial n}{\partial t} = QJ_{\parallel} + S_o - \beta n^2 - \nabla\cdot(n\vec{v}) \tag{1}$$

where Q is the number of ions (per charge) produced by an incident electron per meter, S_o is the source term due to the solar UV radiation and the diffuse auroral precipitation, β ($=10^{-13}$ m^3/sec. Walls et al., 1974) is the recombination coefficient and $J_{\parallel}$ is the field-aligned current density carried electrons. The expression for Q can be approximated by

$$Q = \begin{cases} 0 & J_{\parallel} \text{ downward or } |J_{\parallel}| < J_o \\ Q_o & J_{\parallel} \text{ upward and } \nabla\cdot\vec{E} > 0 \\ \gamma(|J_{\parallel}|-J_o) & J_{\parallel} \text{ upward, } \nabla\cdot\vec{E} > 0 \text{ and } |J_{\parallel}| < J_c \\ \gamma(J_c-J_o) & J_{\parallel} \text{ upward, } \nabla\cdot\vec{E} > 0 \text{ and } |J_{\parallel}| > J_c \end{cases} \tag{2}$$

where $J_o = 0.08$ $\mu A/m^2$ is the electron thermal flux in the loss cone and

$J_c = 1.6\ \mu A/m^2$ is the saturation current density limited by the electron number density in the source region (Knight, 1973; Fridman and Lemaire, 1980). $Q_o = 7 \times 10^{-3}$ ions per charge per meter for 5.6 kev electrons (Rees, 1963), $\gamma = 10^4$ ions/e-m-A/m^2. The condition $\nabla\cdot\vec{E} < 0$ is required for $\vec{E}_\parallel \neq 0$ (Lyons, 1980) on discrete auroral field lines.

As a first approximation, the conductivity is proportional to the electron number density while the field-aligned current is given by the divergence of ionospheric current. Making use of these two relationships in (1), the height-integrated ionospheric conductivity can be written as (e.g., see Zhu and Kan, 1986)

$$\frac{\partial \Sigma_H}{\partial t} = \frac{HQ}{B_o R}\left[\nabla\Sigma_H\cdot(\vec{E}_i + R\hat{B}_o \times \vec{E}_i) + \Sigma_H \nabla\cdot\vec{E}_i\right] + \frac{\beta}{e}\left(\frac{B_o}{H}\right)(\Sigma_o^2 - \Sigma_H^2) - \frac{\hat{B}_o \times \vec{E}_i}{B_o}\cdot\nabla\Sigma_H \qquad (3)$$

where H (=7 km for 5.6 kev electrons) is the effective height of the conducting ionosphere, Σ_o the background conductivity due to solar UV radiation and diffuse auroral precipitation, B_o is the geomagnetic field in the ionosphere and $R = \Sigma_H/\Sigma_P$ which will be assumed to be independent of the energy of the precipitating electrons. The last term in (3) comes from the $\nabla\cdot(n\vec{v})$ term in (1) after making use of the fact that $\nabla\cdot(n\vec{v}) = 0$ in the ionosphere where $\vec{B} = \vec{B}_o$ = constant. Note that the second term in the square brackets is at least one order of magnitude greater than the last term in (3), i.e., HQ > 10 for electron energy greater than 1 kev. Thus, the last term can be neglected in (3) as long as the auroral electron energy is 1 kev or more.

3. Numerical Procedure

The relation between incident wave field and reflected wave field can be expressed as (e.g., Kan and Sun, 1985)

$$(\Sigma_A+\Sigma_P)\nabla\cdot\vec{E}^r + (\nabla\Sigma_P-\hat{B}_o x\nabla\Sigma_H)\cdot\vec{E}^r = (\Sigma_A-\Sigma_P)\nabla\cdot\vec{E}^i - (\nabla\Sigma_P-\hat{B}_o x\nabla\Sigma_H)\cdot\vec{E}^i \qquad (4)$$

where $\Sigma_A = (\mu_o V_A)^{-1}$ is the characteristic conductance of the plasma in the Alfvén wave, $\vec{E}_i$ and $\vec{E}^r$ are the electric fields of incident and reflected Alfvén waves respectively, and B_o is the unit vector of the magnetic field in the ionosphere.

By specifying the reflection coefficient R_m, the Alfvén transit time $T(=L/V_A)$, the initial ionospheric conductivity and the initial enhanced convection field $\vec{E}^{io}$, one can compute the time dependent ionospheric electric field, ionospheric current, ionospheric conductivity, field-aligned currents and the energy flux from equations (2), (3) and (4).

Numerical procedure for solution can be summarized as follows:

(a) The reflected wave field $\vec{E}^r$ from the ionosphere is determined by the numerical solution of (4) using the initial ionospheric conductivity and the initial field $\vec{E}^i(t=0)$. Here $\vec{E}^i(t)$ consists of two parts, that can be written as

$$\vec{E}^i(t) = \vec{E}^{io} + \vec{E}^{il}(t) \qquad (5)$$

where $\vec{E}^{io}$ is the field of the enhanced magnetospheric convection and is assumed to be a step function in time in our model, $\vec{E}^{il}(t)$ is the reflected wave field from the magnetosphere and can be written as

$$\vec{E}^{il}(t) = \begin{cases} 0 & t < 2T \\ \vec{E}^r(t-2T)R_m & t \geq 2T \end{cases} \qquad (6)$$

(b) The ionospheric electric field is the sum of the incident wave field and the reflected wave field. From the electric field and the initial conductivity, we calculate the ionospheric current, field-aligned current and precipitating energy flux.

(c) The conductivity is updated by the numerical solution of (2) and (3) based on the ionospheric electric field and the conductivity of the previous time step.

(d) Using updated conductivity and the updated incident wave field $\vec{E}^i(t=\Delta t)$ determined from equations (5) and (6), the reflected wave field $\vec{E}^r$ of the next time step is determined from equation (4). Then the ionospheric current, the field-aligned current and the energy flux are updated.

Repeat steps (a) through (d), quantities of the model can be updated systematically in time.

4. Results

The inputs of the model are shown in Figure 1. Panel (A) shows the ionospheric projection of the enhanced convection in the magnetosphere, panel (B) shows the input conductivity model, panel (C) and (D) show the distribution of the magnetospheric reflection coefficient. The Alfvén transit time $T(=L/V_A)$ is assumed to be 2 minutes for all field lines throughout the following numerical calculations. These inputs are the same as in the Kan-Sun (1985) model. Figure 2 shows the snapshots of the ionospheric convection pattern at (A) t=32 sec, (B) t=356 sec, (C) t=716 sec and (D) t=1096 sec while it approaches steady state asymptotically. The characteristic distortion leading to the formation of the Harang discontinuity is clearly seen. Figure 3, 4 and 5 show the snapshots of the conductivity distribution, the ionospheric electrojets and the field-aligned currents, respectively. Note that the Region II field-aligned

current is reasonably well reproduced in Figure 5 (D). This is consistent with the finding that the Region II field-aligned current depends primarily on the latitudinal gradient of the ionospheric conductivity (Cheng et al., 1986). This is evident in Figures 3 and 5 where the conductivity gradient increases, the Region II field-aligned current density also increases.

The new results, due to the coupling between the ionospheric time scale and the magnetospheric time scale in the model, are:

(1) The polar cap potential difference in the ionosphere oscillates as it increases toward the enhanced magnetosphere convection level. The average rate of increase of the polar cap potential is a decreasing function of time. These behaviors of the polar cap potential are shown in Figure 6. The oscillations in the polar cap potential are due to the interaction between the two time scales. The potential difference increases on the Alfvén time scale upon magnetospheric convection. Accompanying each enhancement of the potential difference, the field-aligned current density increases which leads to a conductivity enhancement on the ionospheric recombination time scale. The potential difference is found to decrease as the conductivity increases. The above qualitative description explains why the polar cap potential oscillates irregularly as it rises toward the enhanced convection level.

(2) The westward traveling surge moves mainly in the westward direction, but has a small northward component as shown in Figure 7. The westward speed is about 6 km/sec initially and then decreases haltingly. The northward speed reaches up to 1 km/sec for a short time duration, but most of the time is near zero. The variable speeds in the surge motion can be understood as a consequence of the "interaction" between the magnetospheric Alfvén time scale and the ionospheric recombination time scale. The Alfvén time scale is about two minutes, and the recombination time scale is about ten seconds. Qualitatively

speaking, shorter time scale leads to faster speed and vice versa. It follows that the surge on one hand tends to move fast under the ionospheric recombination time scale, but on the other hand is forced to slow down by the magnetospheric Alfvén time scale. As a result, the surge moves at irregular speeds.

In addition, our results also show the development of the Harang discontinuity and the intensification of substorm current wedge as described below:

The distortion of the convection pattern (Heppner, 1977; Evans et al., 1980) is characterized by the Harang discontinuity in the pre-midnight sector. The observed characteristics of the convection pattern is well simulated by our model as shown in Figure 2. According to our model, the Harang discontinuity forms because the ionospheric conductivity is anisotropic and the magnetosphere is not a constant voltage source except on open field lines deep inside the polar cap. The divergence of the Hall current propagates along field lines by Alfvén waves in which the wave electric field is the polarization field generated by the space charge produced from the field-aligned current. As a result the divergence of the Hall current is counter balanced by the divergence of the Pedersen current of the polarization electric field. In this sense the Hall current is said to be blocked from diverging along field lines (Kan and Kamide, 1985).

The substorm current wedge is a three-dimensional current system inferred from observations in which the auroral electrojet currents are connected to the cross-tail plasma sheet current by field-aligned currents (e.g. Clauer and McPheron, 1974; Barfield et al., 1986).

The ionospheric current in Figure 4 and the field-aligned current in Figure 5 are self-consistent with the convection field in Figure 2. In our model, the intensification of the auroral electrojets (Kamide and Akasofu, 1976) goes hand-in-hand with the intensification of the Region I field-aligned

current (Iijima and Potemra, 1976). The region II field-aligned current is under-represented in our model. The three-dimensional current system in our model is driven exclusively by the convection electric field which we believe is fully responsible for the Region I field-aligned current and partially for the region II current. On the dayside, the field-aligned current is centered around the boundary between sunward and anti-sunward convection which corresponds to the low-latitude boundary layer dynamo region (Eastman et al., 1976). On the nightside, the situation is much more complicated. A few minutes after the enhancement of magnetospheric convection, the upward field-aligned current in the pre-midnight sector is centered around the convection reversal boundary as is on the dayside. As the current intensifies, the center of the upward current in the pre-midnight sector shift poleward into the anti-sunward convection region between 70° and 80° latitudes where $-1 < R_m < 0$ which is still on closed field lines. From our model, the substorm current wedge is caused by the enhanced electric field impressed on the ionosphere which intensifies the electrojets first. As the electrojet intensifies, it calls for more field-aligned currents which are drawn from the cross-tail plasma-sheet current. According to our model, the substorm current wedge intensifies not because the cross-tail current is interrupted by some plasma instability processes. It intensifies because the ionosphere demands more field-aligned currents which are drawn from the cross-tail current in the plasma sheet.

It should be noted that the upward field-aligned currents are located where the space charges are negative. This is evident by comparing the convection pattern and the field-aligned current in Figures 4.4 and 4.6. It is seen that the upward field-aligned current in the pre-midnight sector occurs where the convection streamlines rotate clockwise corresponding to negative space charge. This is consistent with the observations that the space charge is

negative at the head of the westward traveling surge where the field-aligned current is upward (Inhester et al., 1981).

In conclusion, we have shown that the interaction of the magnetospheric Alfvén time scale and the ionospheric recombination time scale leads to the irregular oscillations in the polar cap potential difference and in the motion of the westward traveling surge. These irregular oscillations are believed to be a general property of multi-time-scale problems.

Acknowledgement. This work was supported in part by an Air Force contract F19628-85-K-0012. There were four scientific journal articles produced under this support. They are listed in the references as Zhu and Kan (1986), Kan and Sun (1985), Kan and Kamide (1985) and Cheng et al. (1986).

References

Akasofu, S.-I., Polar and magnetospheric substorms, D. Reidel Publ. Co., Dordrecht-Holland, 1968.

Barfield, J. N., N. A. Saflekos, R. E. Sheehan, R. L. Carovillano, T. A. Potemra, and D. Knecht, Three-dimensional observations of Birkeland currents, J. Geophys. Res., 91, 4393, 1986.

Cheng, Q.C., J.R. Kan, and S.-I. Akasofu, Dependence of region II field-aligned currents on the ionospheric conductivity gradient, Preprint, 1986.

Clauer, C. R., and R. L. McPherron, Mapping the local time-universal time development of magnetospheric substorms using mid-latitude magnetic observations, J. Geophys. Res., 79, 2811, 1974.

Eastman, T. E., E. W. Hones, Jr., S. J. Bame, and J. R. Asbridge, The magnetospheric boundary layer: Site of plasma, momentum and energy transfer from the magnetosheath into the magnetosphere, Geophys. Res. Lett., 3, 685, 1976.

Evans, J. V., J. M. Holt, W. L. Oliver, and R. H. Wand, Millstone Hill incoherent scatter observations of auroral convection over $60° \leq \Lambda \leq 75°$, 2. Initial results, J. Geophys. Res., 85, 41, 1980.

Fridman, M., and J. Lemaire, Relationship between auroral electron fluxes and field-aligned electric potential difference, J. Geophys. Res., 85, 664, 1980.

Heppner, J. R., Empirical models of high latitude electric field, J. Geophys. Res. 82, 1115, 1977.

Iijima, T., and T. A. Potemra, Large-scale characteristics of field-aligned currents associated with substorms, J. Geophys. Res., 81, 3999, 1976.

Inhester, B., W. Baumjohnann, R. A. Greenwald, and E. Nielsen, Joint two-dimensional observations of ground magnetic and ionospheric electric fields associated with auroral zone currents, 3, Auroral zone currents during the passage of a westward traveling surge, J. Geophys. Res., 49, 155, 1981.

Kamide, Y., and S.-I. Akasofu, The auroral electrojet and field-aligned current, Planet. Space Sci., 24, 203, 1976.

Kan, J. R., and Y. Kamide, Electrodynamics of the westward traveling surge, J. Geophys. Res., 90, 7615, 1985.

Kan, J.R., and W. Sun, Simulation of the westward traveling surge and Pi2 pulsations during substorms, J. Geophys. Res., 90, 10911, 1985.

Knight, S., Parallel electric fields, Planet. Space Sci., 21, 741, 1973.

Lyons, L.R., Generations of large-scale regions of auroral currents, electric potentials, and precipitation by the divergence of the convection electric field, J. Geophys. Res., 85, 17, 1980.

Rees, M.H., Auroral ionization and excitation by incident energetic electrons, Planet. Space Sci., 11, 1209, 1963.

Rothwell, P.L., M.B. Silevitch and L.P. Block, A model for the propagation of the westward traveling surge, J. Geophys. Res., 89, 8941, 1984.

Vasyliunas, V. M., The interrelationship of magnetospheric processes, in Earth's Magnetospheric Processes, ed. by McCormac, p. 29, D. Reidel, Dordrecht-Holland, 1972.

Walls, F.L., and G.H. Dunn, Measurement of total cross-section for electron recombination with NO^+ and O_2^- using ion storage technology, J. Geophys. Res., 79, 1911, 1974.

Zhu, L., and J.R. Kan, Time evolution of the westward traveling surge on an ionospheric time scale, Planet. Space Sci., (in press), 1986.

Figure Captions

Figure 1. (A) Equipotential contours of the input potential Fo. (B) Contours of the input Hall conductivity. (C) Contours of the reflection coefficient Rm at magnetospheric source regions projected along field lines onto the polar ionosphere. (D) Latitudinal dependence of Rm along the noon-midnight meridian.

Figure 2. Temporal evolution of the ionospheric convection patterns at (A) t=32 sec, (B) t=356 sec, (C) t=716 sec and (D) t=1096 sec.

Figure 3. Temporal evolution of the ionospheric Hall conductivity.

Figure 4. Temporal evolution of the ionospheric electrojets.

Figure 5. Temporal evolution of the field-aligned currents.

Figure 6. Time variation of the polar cap potential difference

Figure 7. Time variation of the westward and the northward displacements of the westward traveling surge.

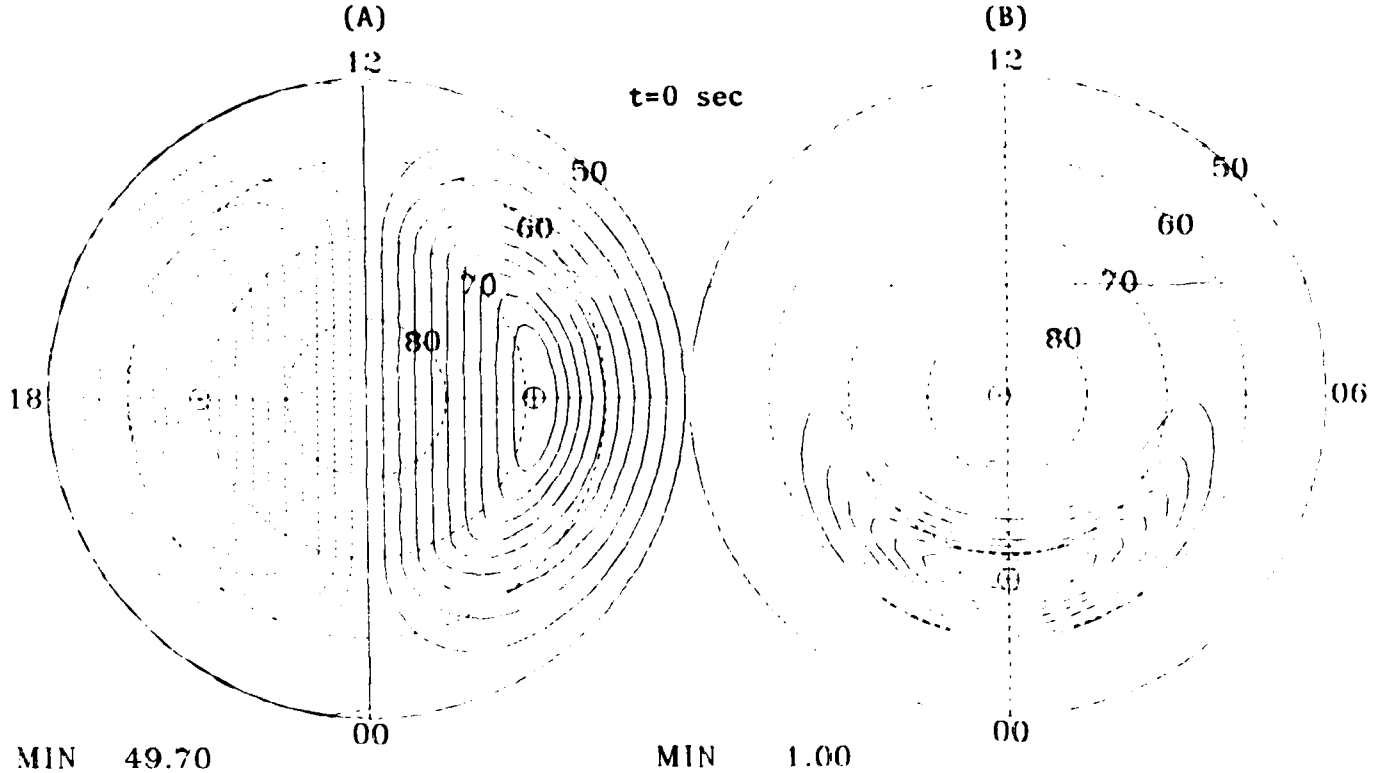

MIN 49.70
MAX 49.70
CONTOUR INTERVAL 5.00 KV

MIN 1.00
MAX 15.03
CONTOUR INTERVAL 2.00 MHO

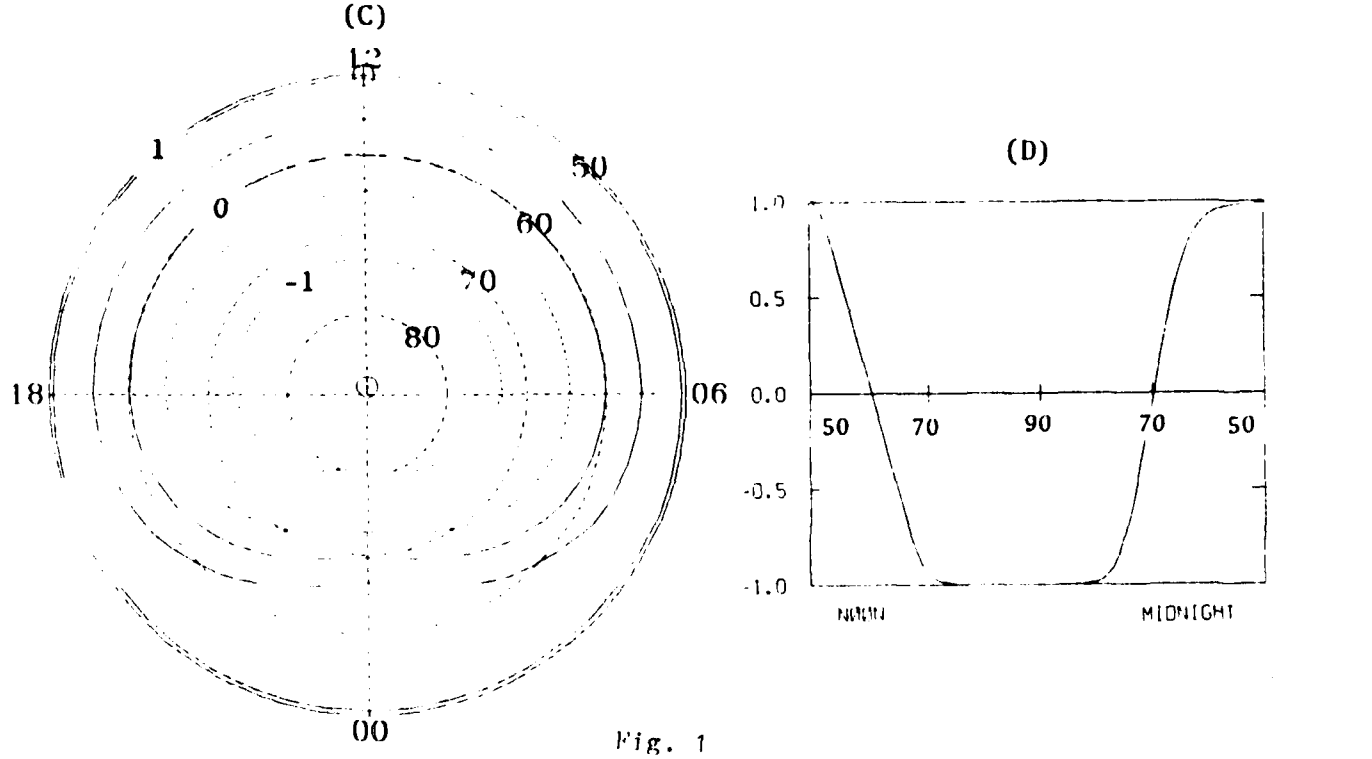

Fig. 1

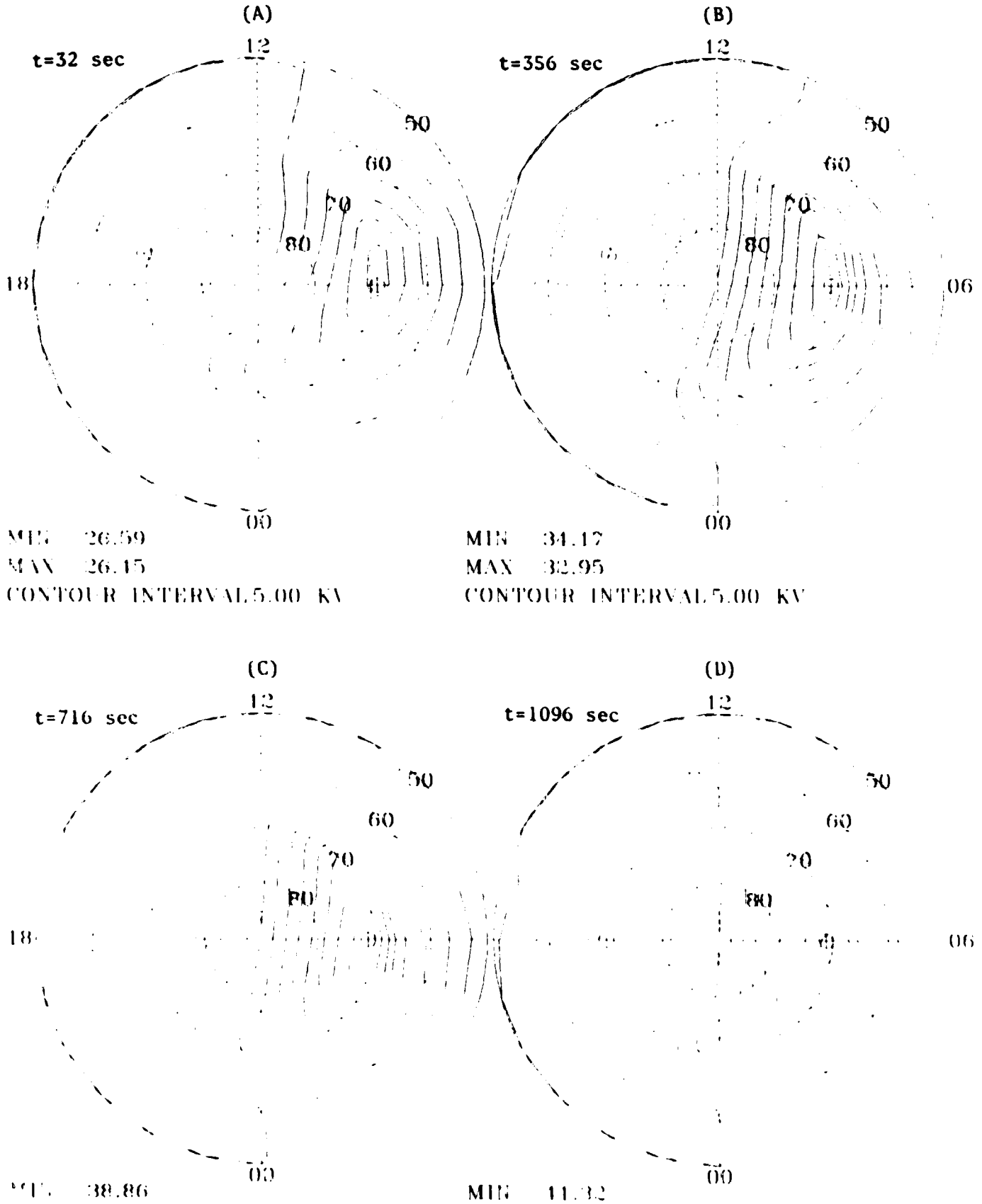
(A)
t=32 sec
12
50
60
70
80
18
00
MIN 26.59
MAX 26.15
CONTOUR INTERVAL 5.00 KV
(B)
t=356 sec
12
50
60
70
80
06
00
MIN 34.17
MAX 32.95
CONTOUR INTERVAL 5.00 KV
(C)
t=716 sec
12
50
60
70
80
18
00
MIN 38.86
MAX 38.33
CONTOUR INTERVAL 5.00 KV
(D)
t=1096 sec
12
50
60
70
80
06
00
MIN 11.32
MAX 10.81
CONTOUR INTERVAL 5.00 KV

Fig. 2

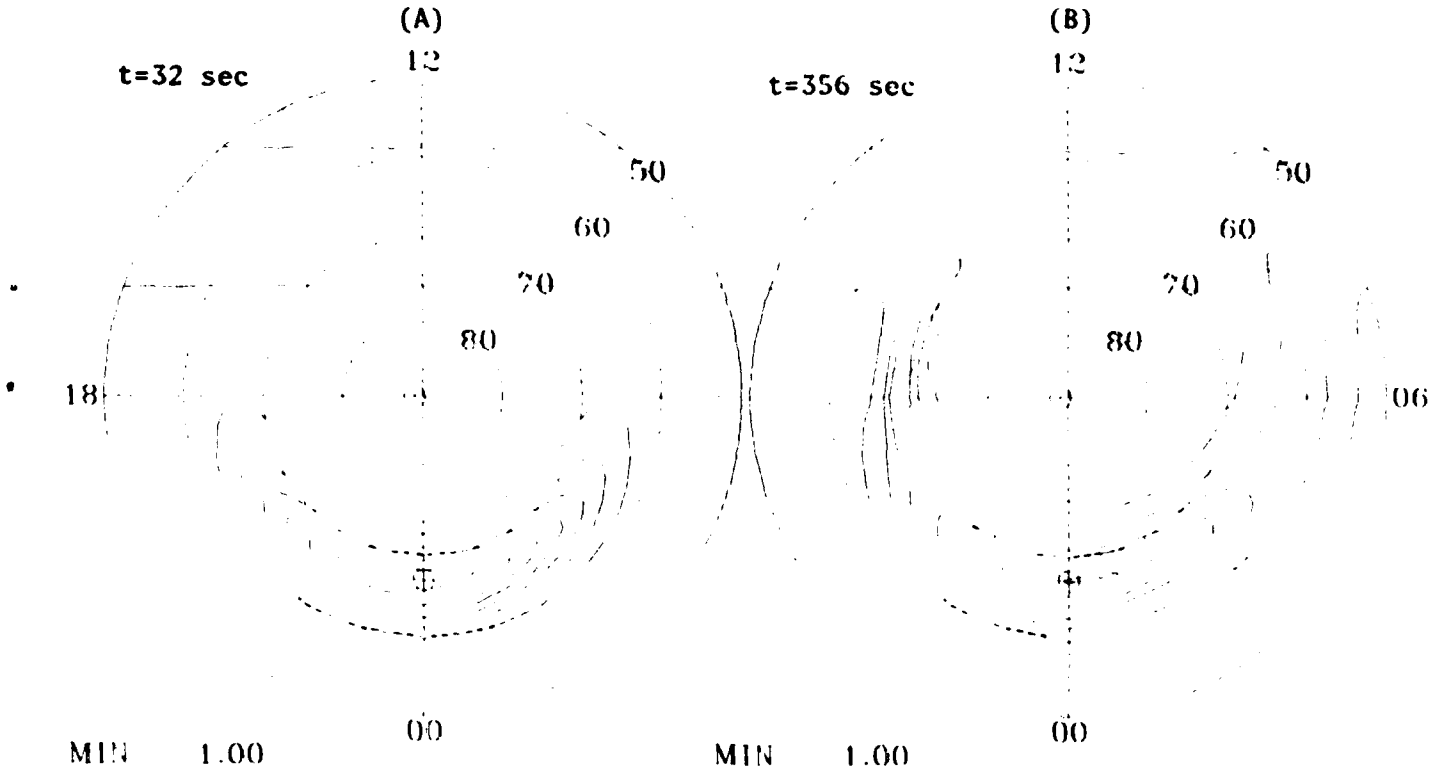

MIN 1.00
MAX 15.03
CONTOUR INTERVAL 2.00 MHO

MIN 1.00
MAX 14.13
CONTOUR INTERVAL 2.00 MHO

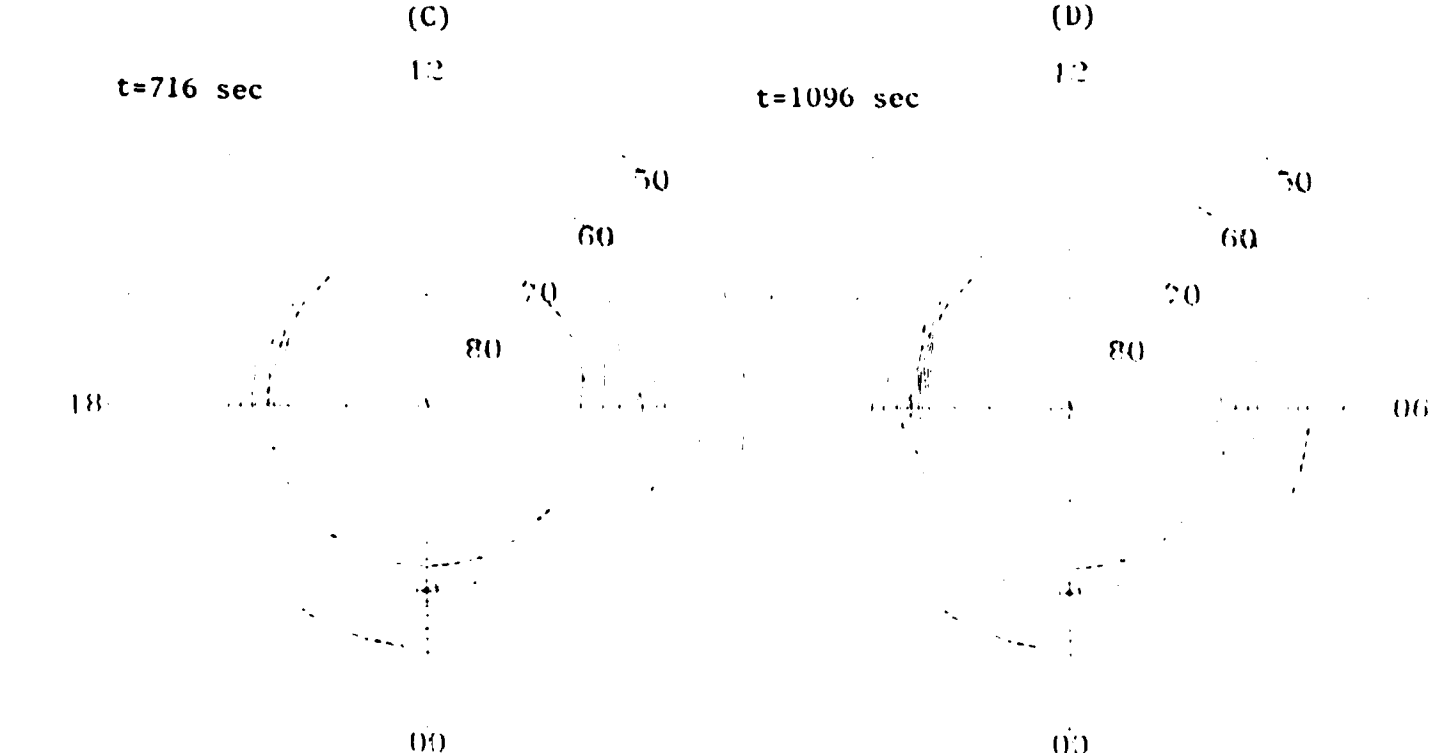

MIN 1.00
MAX 14.13
CONTOUR INTERVAL 2.00 MHO

MIN 1.00
MAX 14.13
CONTOUR INTERVAL 2.00 MHO

Fig. 3

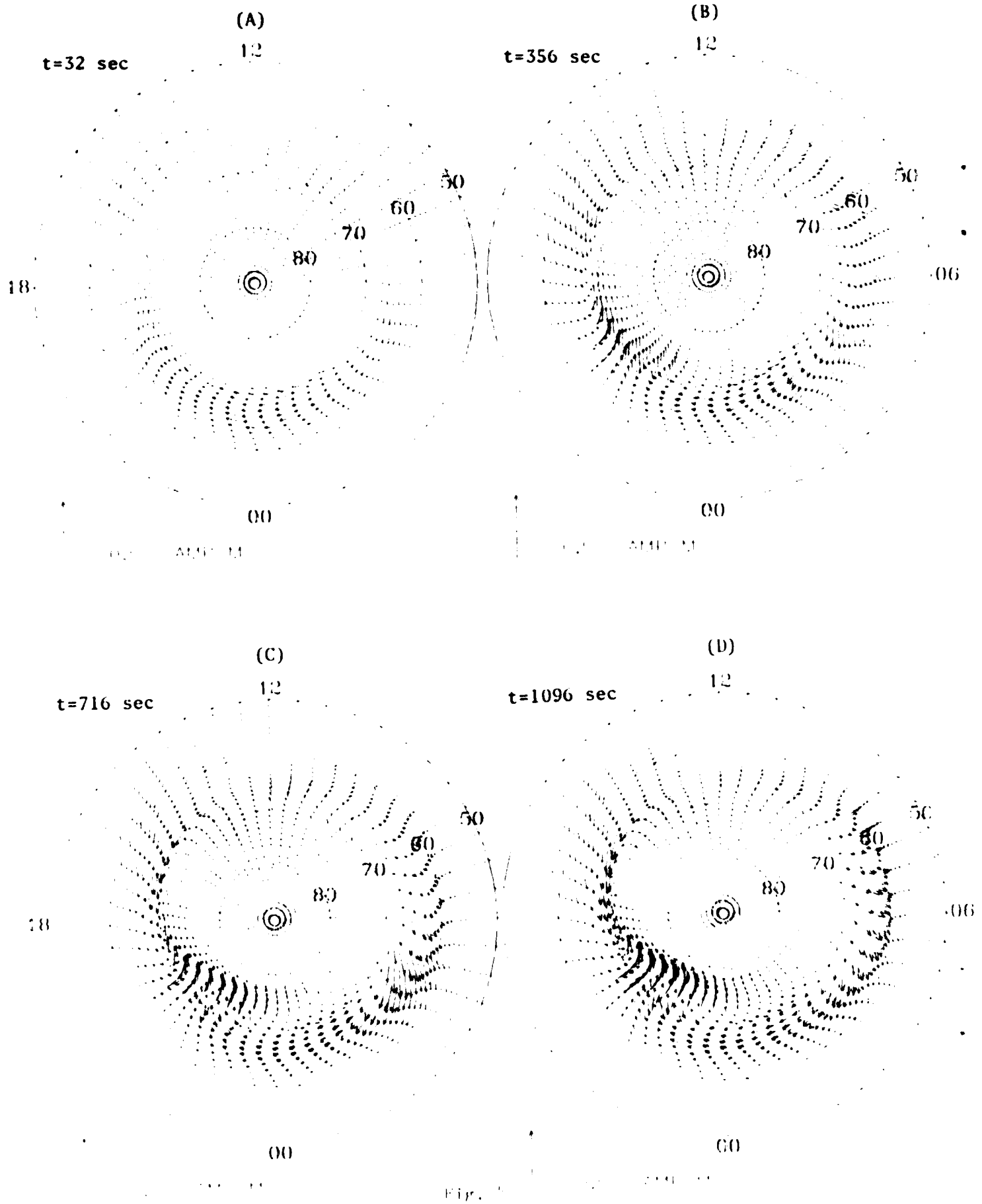
(A)
t=32 sec
12
50
60
70
80
18
00
(B)
t=356 sec
12
50
60
70
80
06
00
(C)
t=716 sec
12
50
60
70
80
18
00
(D)
t=1096 sec
12
50
60
70
80
06
00

Fig.

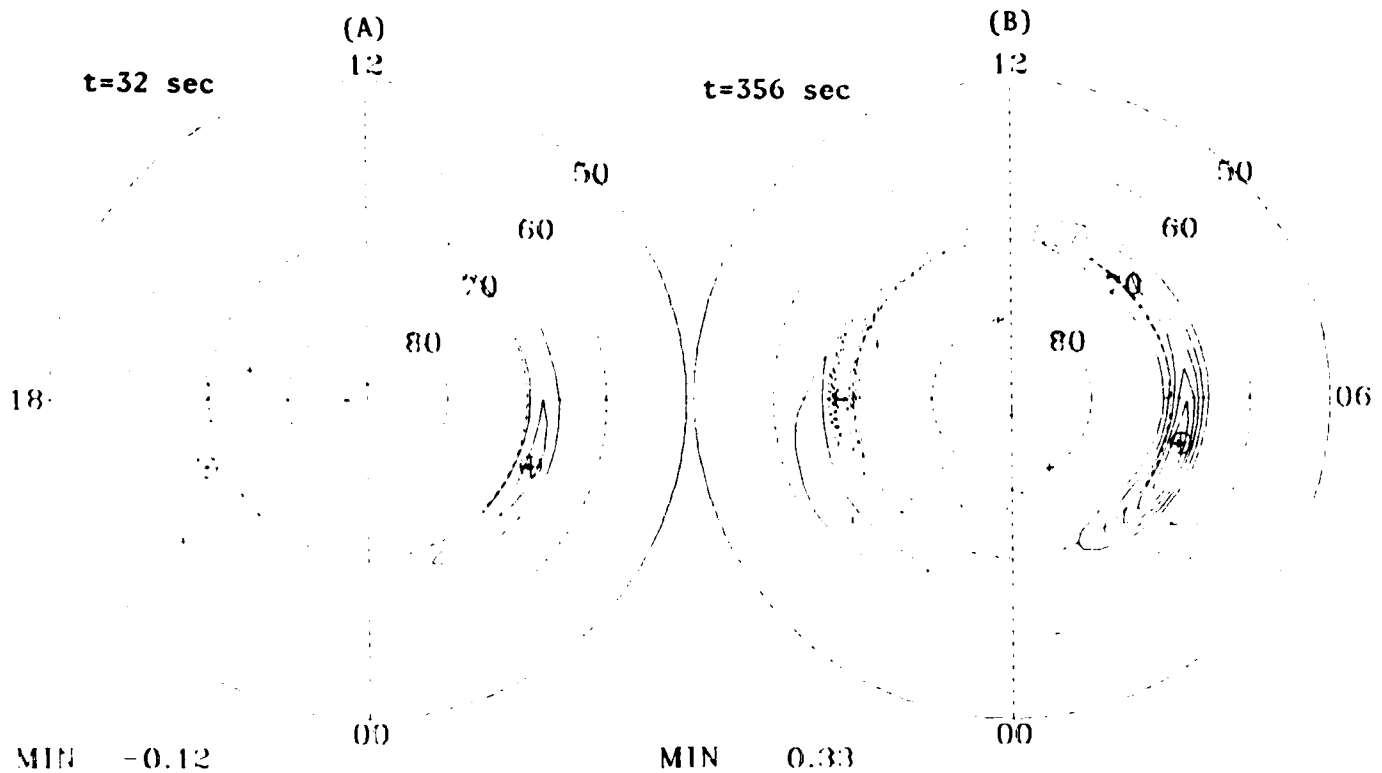
(A)
t=32 sec
12
50
60
70
80
18
00
MIN -0.12
MAX 0.12
CONTOUR INTERVAL 0.05 μA m⁻²
(B)
t=356 sec
12
50
60
70
80
06
00
MIN 0.33
MAX 0.29
CONTOUR INTERVAL 0.05 μA m⁻²

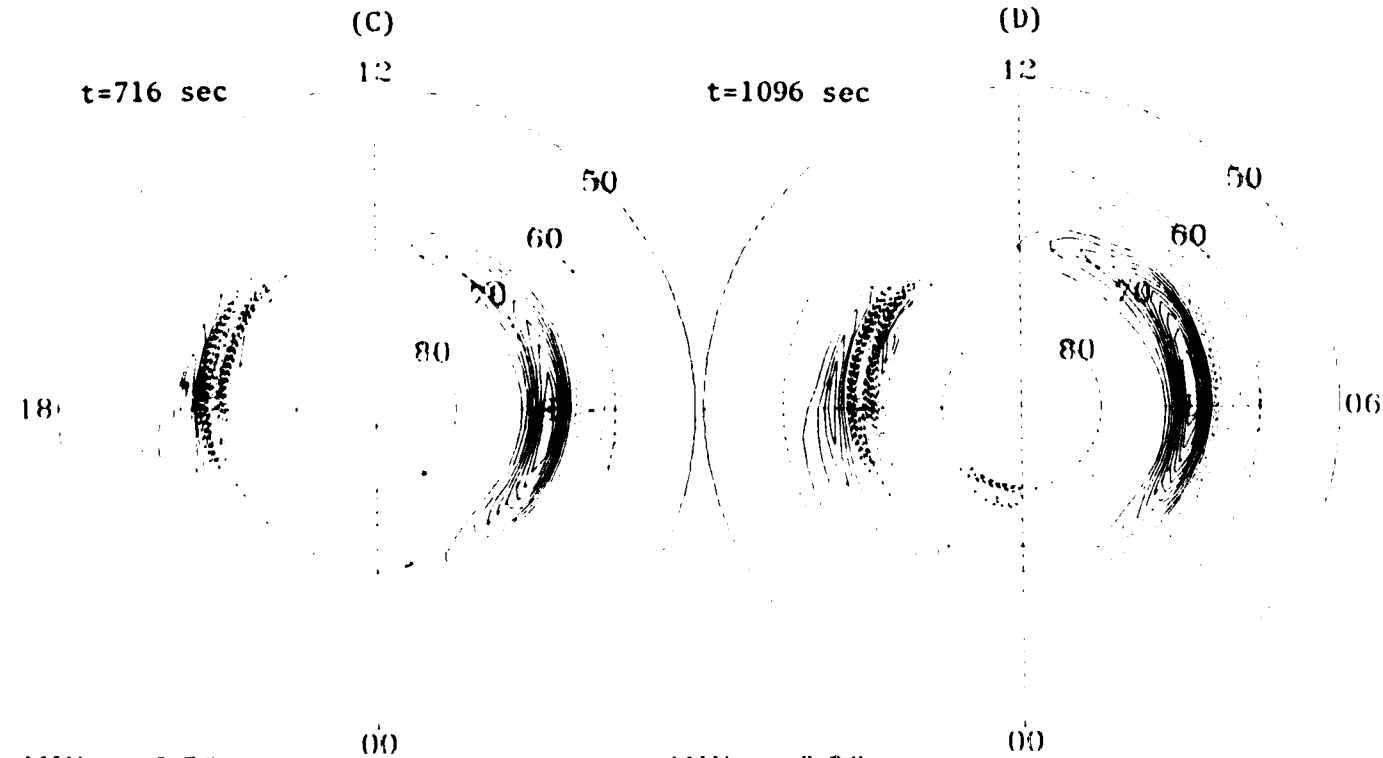
(C)
t=716 sec
12
50
60
70
80
18
00
MIN 0.59
MAX 0.45
CONTOUR INTERVAL 0.05 μA m⁻²
(D)
t=1096 sec
12
50
60
70
80
06
00
MIN 0.70
MAX 0.60
CONTOUR INTERVAL 0.05 μA m⁻²

Fig. 5

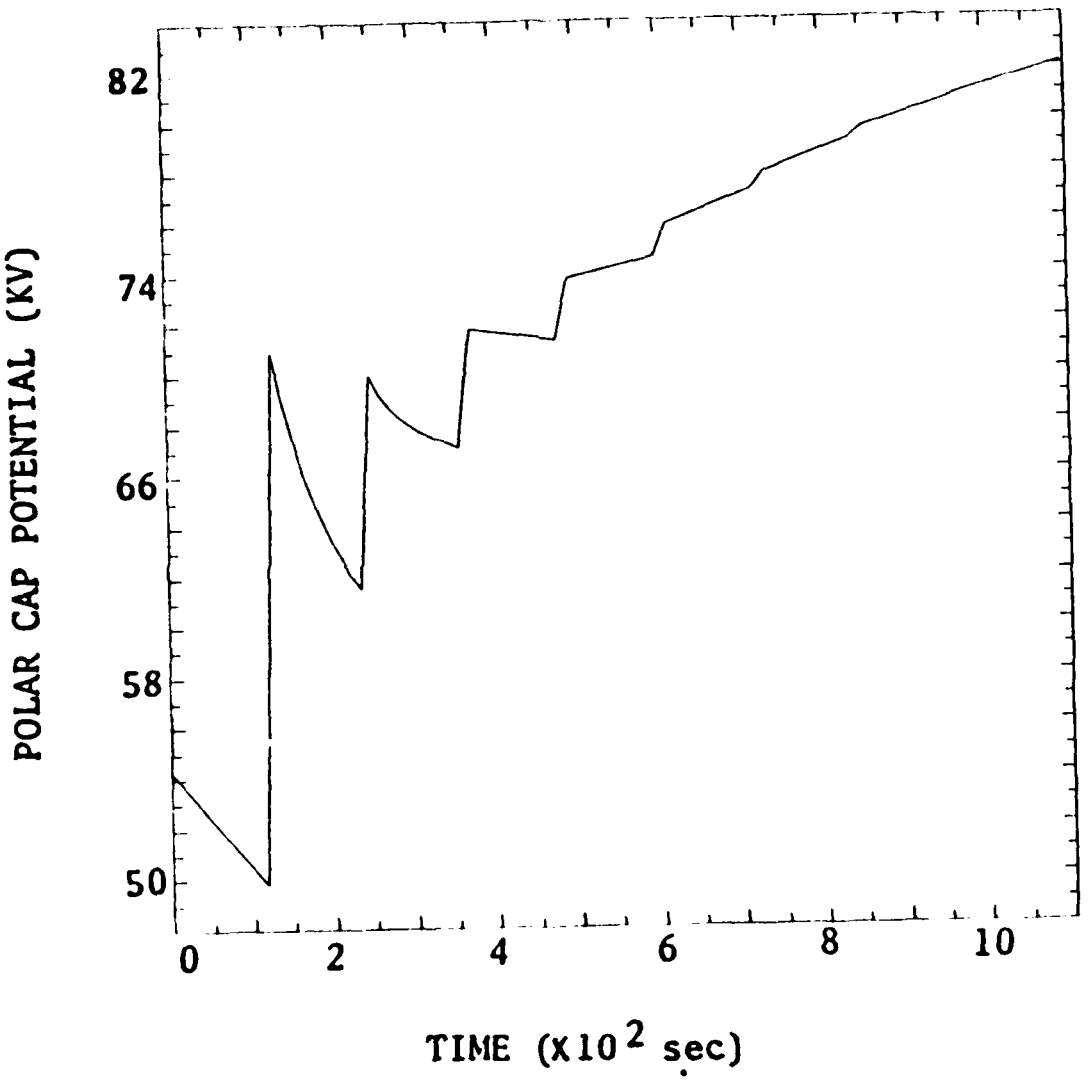

Fig.6

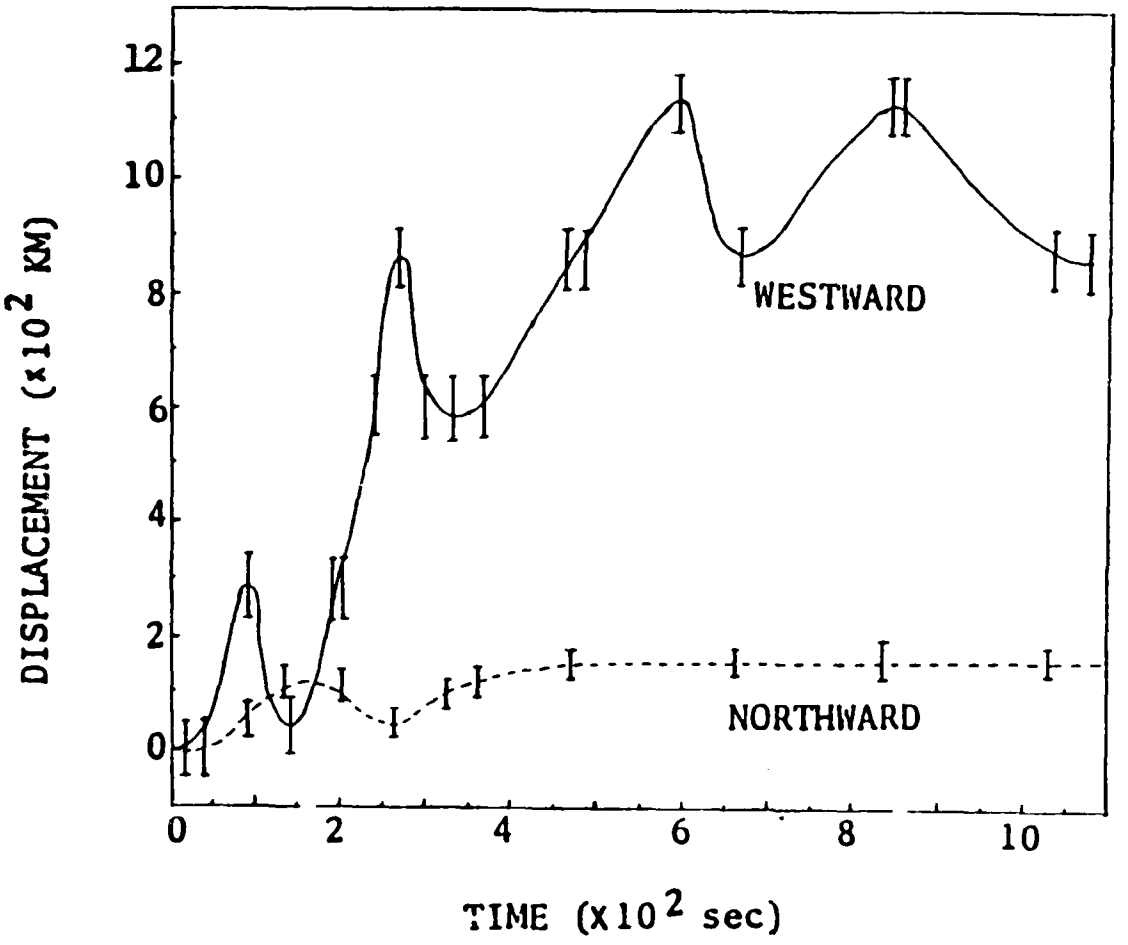
DISPLACEMENT (x10^2 KM)
12
10
8
6
4
2
0
WESTWARD
NORTHWARD
0
2
4
6
8
10
TIME (X10^2 sec)

Fig.7

END

6-87

DTIC